IJMMM International Journal of Minerals, Metallurgy and Materials 矿物冶金与材料学报（英文版）

Synthesis of crystal-phase and color tunable mixed anion co-doped titanium oxides and their controllable photocatalytic activity

Jingdi Cao, Takuya Hhasegawa, Yusuke Asakura, Akira Yamakata, Peng Sun, Wenbin Cao, and Shu Yin

Cite this article as:
Jingdi Cao, Takuya Hhasegawa, Yusuke Asakura, Akira Yamakata, Peng Sun, Wenbin Cao, and Shu Yin, Synthesis of crystal-phase and color tunable mixed anion co-doped titanium oxides and their controllable photocatalytic activity, *Int. J. Miner. Metall. Mater.*, 30(2023), No. 10, pp. 2036-2043. https://doi.org/10.1007/s12613-022-2573-6

View the article online at SpringerLink or IJMMM Webpage.

International Journal of Minerals, Metallurgy and Materials
Volume 30, Number 10, October 2023, Page 2036
https://doi.org/10.1007/s12613-022-2573-6

Synthesis of crystal-phase and color tunable mixed anion co-doped titanium oxides and their controllable photocatalytic activity

Jingdi Cao[1)], *Takuya Hhasegawa*[1)], *Yusuke Asakura*[2)], *Akira Yamakata*[3)], *Peng Sun*[1,4)], *Wenbin Cao*[4)], *and Shu Yin*[1,5),✉]

1) Institute of Multidisciplinary Research for Advanced Materials, Senda 980-8577, Japan
2) Kagami Memorial Research Institute for Materials Science and Technology, Waseda University, Shinju-ku 169-0051, Japan
3) Graduate School of Natural Science and Technology, Okayama University, Okayama 700-8530, Japan
4) University of Science and Technology Beijing, Beijing 100083, China
5) Advanced Institute for Materials Research (WPI-AIMR), Tohoku University, Sendai 980-8577, Japan
(Received: 8 September 2022; revised: 14 October 2022; accepted: 15 November 2022)

Abstract: B and N mixed anions co-doped titania with various crystal phases such as anatase, brookite, and rutile were successfully synthesized by a hydrothermal synthesis followed by heat treatment in an ammonia gas atmosphere at 550–650°C (denoted as BN-Ana_*x*, BN-Bro_*x*, and BN-Rut_*x*, *x* is the treatment temperature). The colors of as-prepared BN-Ana, BN-Bro, and BN-Rut are red, yellow-green, and cyan-green, respectively. The color changing mechanism of titania was related to their various band gap structure and the existence of B–N bonding. The nitridation temperature exhibits effective color changing compared to that of nitridation time. The different phases of the mixed anion co-doped titania possess different photocatalytic deNO_x activity. The BN-Ana and BN-Rut show poor photocatalytic deNO_x activity, while the BN-Bro shows excellent photocatalytic deNO_x activity, better than that of standard titania photocatalyst Degussa P25. The colorful titania with low-photocatalytic activity is heavy metal elements free, indicating their possible applications as nontoxic color pigments or novel cosmetic raw materials.

Keywords: colorful titania; toxic elements free; mixed anion compounds; pigment; photocatalytic activity; cosmetic application

1. Introduction

Functionality design and its synthesis process have attracted great attention from researchers. The physical and chemical properties of inorganic functional materials changed greatly with their composition, crystal structure, morphologies, and particle size, resulting in many potential applications such as photocatalysts, gas sensors, pigments, smart windows, and so on [1–10]. Facing worldwide energy shortage and serious environmental issue, the development of sustainable green energy has become a current topic of intensive interest. To reduce the dependency on fossil fuels, there is an urgent demand for alternative energy technology in the present 21th century [11]. The energy originated from natural sources, for instance, sunlight, wind, biology, geothermal heat, and so on [12–13], are defined as green energy because they are renewable, eco-friendly, and relatively infinite compared to conventional fossil fuels (petroleum, coal, and natural gas). In order to utilize solar energy effectively, semiconductor photocatalyst is one of the vital mediums that can inherit the energy from light and subsequently apply it to the chemical reactions, namely, catalyze the process of light-electricity conversion. Titanium dioxide (TiO_2) is a potential and prevalent photocatalyst for the decomposition of environmental pollutants under ultraviolet (UV) light irradiation, but its disadvantage, being inert to solar light, represents the major obstacle greatly precluding the practical application of TiO_2 as an efficient visible-light photocatalyst. Recently, various photocatalytic materials have been applied to environmental purification. Many studies have been conducted to improve photocatalytic activity by co-doping [4–5,14–19], the formation of composite [20–25], and some novel catalyst systems [25–27]. Although co-doping with cations and anions is the mainstream [5,16–17], mixed-anion co-doping (such as boron, nitrogen, and sulfur etc.) have also attracted the researcher's attention [4,14–15,19]. As one of the solving strategies for titanium oxide materials, inserting isolated mid-state into the bandgap by impurity doping has attracted considerable attention over the recent years. Generally, the purpose of inducing extrinsic elements into the framework of TiO_2 is to create trap levels either below the conduction band (CB) or beyond the valence band (VB). Since those newly formed defective levels result in a relatively smaller bandgap compared with original TiO_2 (3.0–3.2 eV), the enhanced sol-

✉ Corresponding author: Shu Yin E-mail: yin.shu.b5@tohoku.ac.jp

ar light absorption ability has been expected. Unfortunately, it is still ambitious that the absorption threshold cannot be modulated evidently by doping impurity until nowadays. Even the most promising N-doped TiO_2 only presents a weakened absorption toward the light with a wavelength of 450 nm [1,28]. Recently, a kind of reddish B and N co-doped titania (BN-TiO_2) has come into sight [4,14–15]. It was found that the absorption onset could be potentially developed to ca. 700 nm, which is probably the most efficient visible light absorbing TiO_2 derivative. Although the researchers have made great efforts to disclose the secrets of this significant bandgap narrowing as the gradient distribution of B and N dopants in the radial direction, there are still numerous unexplained mysteries remaining. Particularly, the photocatalytic activity dependences of different crystal compositions of TiO_2 with various colors have not been studied well.

Besides photocatalyst, TiO_2 is also an irreplaceable source of traditional white pigment and cosmetic raw materials. TiO_2 is stable and inert, but their photocatalytic activity is poor, such as part of UV light leads to the degradation of organic pigments or the binder and the chalking of paint films. In a word, the widely used TiO_2 as a traditional pigment and cosmetic material also shows some disadvantages and needs to be further studied. In the present research, we successfully synthesized BN-TiO_2 in anatase, rutile, and brookite phases corresponding to red, cyan-green, and yellow-green apparent color, respectively. Also, the photocatalytic performance of BN-TiO_2 are further investigated.

2. Experimental

The B-doped titania was synthesized by previous reports [4,14,29]. 1.1118 g of TiB_2 was added into 80 mL of (i) 0.5 M Na_2SO_4/0.5 M H_2SO_4 solution, (ii) DL-sodium lactate solution together with 9.6089 g urea, and (iii) 0.5 M HCl solution for the products of anatase, brookite, and rutile phases. Then, N doping was carried out by heat treatment in NH_3 atmosphere at 500–700°C for 1 h with a flow rate of 50 mL·min^{-1}. The colorful titania was denoted as BN-Ana_*x*, BN-Bro_*x*, and BN-Rut_*x* (*x* is the treatment temperature), respectively. The typical synthesis process is illustrated in Scheme S1.

The phase composition of the titania was characterized by X-ray diffraction (XRD, Bruker AXS D2 Phaser, Cu K_α). The UV-vis spectra were recorded by a UV-vis spectrophotometer (JASCO V-670) with an integrating sphere. A color reader (CR-20, Konika-Minolta) was utilized to characterize the CIELAB system of the color powders [30]. For the transient absorption spectrum measurement, the calcium fluoride (CaF_2) substrate unfolded by sample powder with a density of 1.5 g·cm^{-3} was prepared. A 450 nm pulse generated from an Nd:YAG laser (Continuum Surelite; duration, 6 ns; power, 5 mJ; repetition rate, 0.1–5 Hz) was used as the pump light to photoexcite target sample. The transient absorption in the range of 20000–6000 cm^{-1} (visible-mid-IR region) was measured in the diffuse-reflection model. The transmission model was applied to record the response in the part of 6000–1000 cm^{-1} by a mercury cadmium telluride (MCT) detector (Kolmar Inc.). All measurements were performed under N_2 atmosphere with a pressure of 2666 Pa. The time resolution of the spectrometer was fixed to 1–2 μs as dictated by the bandwidth of the amplifier (Stanford Research Systems, SR560, 1 MHz). The X-ray photoelectron spectroscopy (XPS) characterization was carried out by ULVAC PHI5600 with a 200 W monochromatic Al K_α X-ray source. The photocatalytic activities were evaluated by light-driven NO gaseous decomposition behaviors. The schematic experimental system was illustrated in Scheme S2. The photocatalytic characterization was carried out by a single tested continuous flowing system, based on a Japanese Industrial Standard ([JIS R 1701-1:2004(J)] [31]. In a typical experiment, a certain number of samples were stabilized on a glass substrate which has a central cell with a size of 20 mm × 16 mm × 0.2 mm. Second, the glass substrate filled with sample powder was fixed to a closed chamber with an internal volume of 373 cm^3. There is a transparent window just above the sample substrate, allowing the entrance of light. Before measurement, it was needed to implement the zero setting to the reaction system by flowing 200 mL·min^{-1} pure N_2 gas and keeping for a few times until the concentration of NO decrease to 0. Third, 200 mL·min^{-1} mixed gas consisting of 2.98×10^{-6} NO and N_2 (based gas) was fed into NO_x analyzer (Yanaco ECL-88A) to calibrate the concentration scale (0–2.98×10^{-6}). After zero setting and scale calibration were finished, the reaction system was ready to carry out the NO photodegradation experiment. The total flux of feed gas was fixed at 200 mL·min^{-1} and the concentration of NO was controlled to around 1.00×10^{-6} as the initial concentration (C_0) by adjusting the relative flow rate of NO/N_2 mixed gas (with 2.02×10^{-6} NO) and compressed air. The outlet gas (after photocatalytic reaction) continued to flow into the NO_x analyzer so that the residual concentration of NO (C_t) could be recorded timely. A 450 W high-pressure mercury lamp was applied as the light source. Three kinds of optical filters, Fuji triacetyl cellulose filter for >510 nm, Kenko L41 Super Pro (W) filter for >400 nm, and Pyrex glass for >290 nm [15], were utilized to selectively cutoff the wavelength of light. The degradation ratio of NO (deNO_x ratio) was calculated as the following equation.

$$\text{de}NO_x \text{ ratio} = \frac{C_0 - C_t}{C_0} \times 100\% \quad (1)$$

The initial concentration of NO (C_0) and concentration of NO at time *t* (C_t) was recorded when the reaction system reached dynamic equilibrium status. Here, a recovery time was set between every illumination experiment in order to ensure the initial amount of NO species was the same, or the difference could be ignored. In actual operation, we kept the reaction chamber under darkness until the concentration of NO returned to 1.00×10^{-6} once again. After that, the sample holder would be exposed to the light again for the next degradation test. The five times cycling successive experiments were performed the same as the above. Typically, five cycles of light off-on were implemented for one cutoff filter.

3. Results and discussion

3.1. Crystal structure and optical properties

The XRD patterns of the BN-TiO_2 nitride by 30, 60, and 120 min together with the standard anatase TiO_2 (PDF No. 65-5714) are shown in Fig. 1. The main crystal compositions of the B/N co-doped titania are anatase, brookite, and rutile, respectively. The time of nitridation showed almost no effect on the phase composition, while there are some impurity peak of TiB_2 appeared in the BNA_120 sample. TiB_2 can be synthesized by the carbothermal reduction of TiO_2–H_3BO_3–C following the reaction equation [32].

$$TiO_2 + 2H_3BO_3 + 5C = TiB_2 + 3H_2O + 5CO \quad (2)$$

where the carbon (C) plays the role of reducing agent to give out one electron to B atom, resulting in +3 to −2. The TiB_2 could be obtained by heating the composite of TiO_2–B_2O_3–Mg, where Mg also enables +3 B transfer to −2 B and eventually forms into TiB_2 [33]. Applying these opinions to understand what happens in the BN-Ana samples during the nitridation treatment, it is possible to consider that in the initial stage of nitridation, most ammonia gaseous are favor of replacing the lattice O in B-TiO_2 with the results of two kinds of N dopants (substitutional N (N_{sub}) and interstitial N (N_{int})) and corresponding Ti^{3+} centers [33]. Meanwhile, with the influence of N doping the intrinsic B_{sub} (approximately 0 charges) gradually shifts to B_{int} (+3) species [34] (Fig. 2). The peak with binding energy smaller than 190 eV corresponds to B_{sub} and another peak with energy *ca*. 192 eV refers to B_{int} [35]. The ratio of B_{sub}/B_{int} overturned after nitridation, namely, the introduction of N is able to increase the amount of B_{int} selectively. The abundance of B_{int} in BN-TiO_2 will be reduced by ammonia gaseous, similar to H_3BO_3 or B_2O_3 in the Eqs. (1) and (2), and eventually formed TiB_2. On the other hand, BN-Rut and BN-Bro remain their crystal structures and no detective TiB_2 impurity even if the nitriding for 120 or 30 min. It is noting that small amount of rutile phase (a peak around 27°) might be found in the brookite phase, as shown in Fig. 1(c).

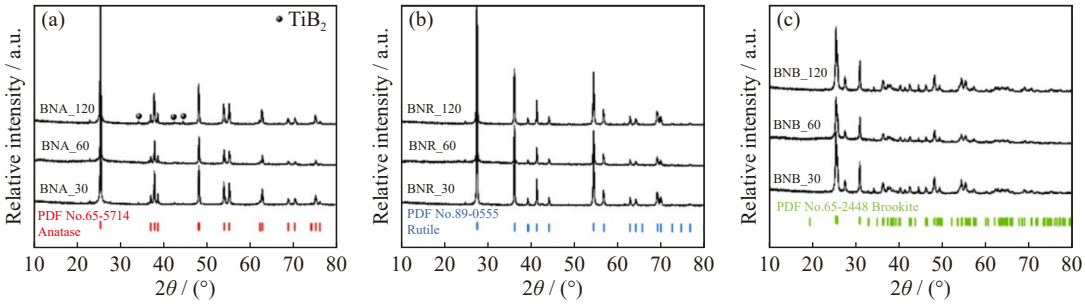

Fig. 1. XRD patterns of the BN-TiO_2 nitride by 30, 60, and 120 min: (a) BN-Ana (BNA); (b) BN-Rut (BNR); (c) BN-Bro (BNB).

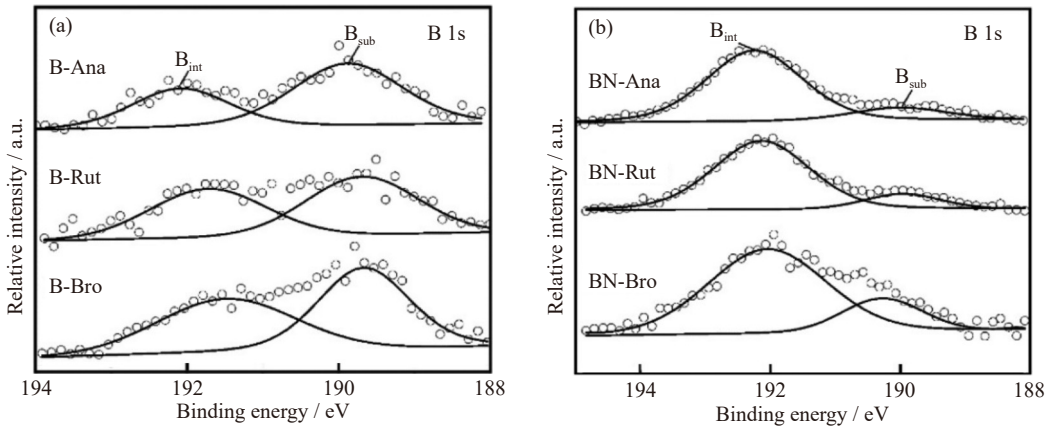

Fig. 2. The B 1s XPS spectra of B 1s of different B-TiO_2 phases (a) before and (b) after nitridation at 600°C for 60 min.

The SEM images of BN-Ana, BN-Rut, and BN-Bro are displayed in Fig. S1. As can be seen, the particles show an agglomeration state with several micrometer in size. Because BN-Ana and BN-Rut are pure phases, the morphologies of almost crystal grains are uniform. Typically, BN-Ana has a morphology of truncated bipyramid, BN-Rut possesses not sharp but rod-like monomers. Both cuboid segments and nanoparticle aggregation have been observed in the case of BN-Bro.

To further interpret the effects of nitridation time on the optical property (coloring), the UV-vis absorption spectra have been measured (Fig. 3). Generally, the nitridation time does not virtually impact the light absorption properties of three BN-TiO_2. The extension of reaction time is only useful for the enhancement of absorption on the long-wavelength side, namely, the extra N dopants are unable to vary the bandgap configurations but just create more Ti^{3+} and strengthen the d–d transition

It was found that the color parameters of BN-TiO_2 (Table S1) barely change whether the crystal phase is anatase, rutile,

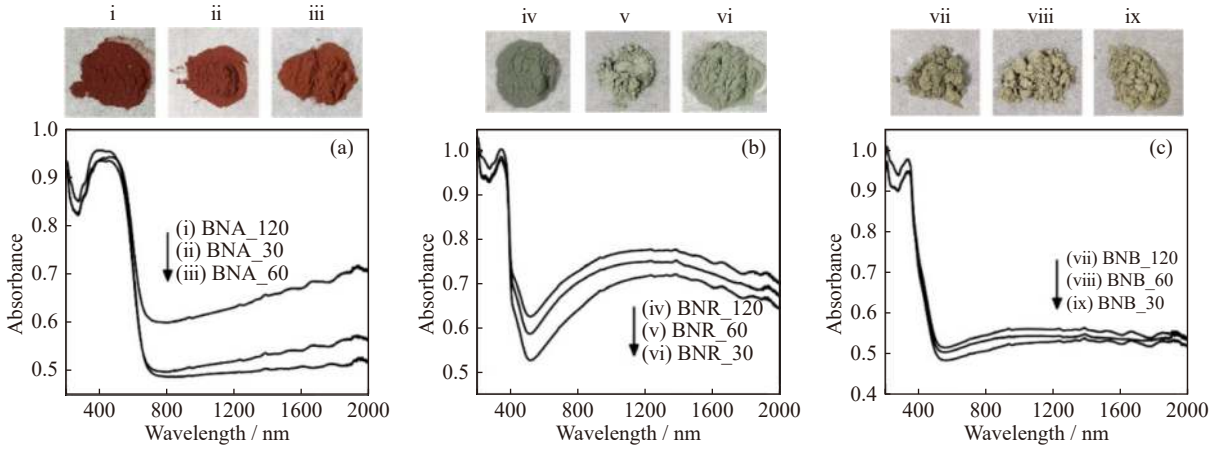

Fig. 3. UV-vis spectra of (a) BNA, (b) BNR, and (c) BNB samples treated at 600ºC for different nitration time. The photographs of corresponding sample are presented.

or even brookite. Particularly, the color hue ($h°$) is a useful indicator to evaluate the deviation between colors. With larger differences between $h°$, the color changes drastically. The $h°$ of BNA samples are around 30, which is the region of red, The $h°$ of BNR has value in the range of cyan (310–320), and the $h°$ of BNB gathers around 295. The detailed movement that occurred in L*a*b* color coordinate (CIELAB color space [4]: L* represents the brightness (black (0) → white (100)); a* (green (–) → red (+)); b* (blue (–) → yellow (+)) represent the color parameter) was collected in Fig. S2 as the function of nitridation time. In our previous research, it was found that the coloring of the mixed anion doped titania is strongly related to the phase composition, the different bandgap configurations, and widely produced hybrid/composite B–N energy level above the valence band maximum (VBM), leading to the formation of covalent B–N bonding and the different amount of Ti^{3+} [4]. It is recognized that N_{sub} shows a trap state above the valence band maximum (VBM) and the N_{int} existed as mid-state [36–37]. The N_{sub} and N_{int} levels contact together to show a continuous and a wide energy state overlaps with the VBM. The N dopants are preferred to be combined with B_{int} in the B element doped anatase and brookite (B-Ana and B-Bro), while the N element in the rutile phase were preferred to remain along. It might be suggested that the interaction between N and B elements in BN-Ana and BN-Bro phases, resulted in a wide hybrid/composite B–N energy level above the VBM [4].

Fig. 4 shows the transient absorption spectra of BN-Ana, BN-Rut, and BN-Bro samples. The 450 nm pump light corresponds to the excitation of electrons in N_{int} state. The signals in BN-Ana spreads over the visible-mid-NIR region, indicating substantial defect energy levels successively spread over the N_{int} state. Two intensive signals at 16200 and 6000 cm^{-1} appeared in the BN-Ana, indicating the existence of deeply trapped holes and shallowly trapped electrons below the CB [38], respectively.

It should be noted that the signal at 19000 cm^{-1}, which is assigned to the hole trapped in the VB [39], is blank. The N doping states serving as a hole trapping center occupy the bottom of the hybrid state. On the other side, the B_{sub} works as an electron trapping level, also connects with the nitrogen level to produce a widely spread band state. The same explanation is also applicable to BN-Bro. Within the bandgap of BN-Rut, only a portion of shallow states exist (4000 cm^{-1}) and no deep state has been obviously detected. The potentially different electronic arrangements and bandgap structures of three TiO_2 offer an idea to comprehend the different colors of anatase, rutile, and brookite TiO_2. As is well known, anatase crystallizes in the tetragonal $I4_1/amd$ space group, rutile structures in the tetragonal $P4_1/mnm$ space group, and brookite structures in the orthorhombic *Pbca* space group [40]. Perhaps these different spatial arrangements are the potential to determine the optimum configuration [41] for B and N co-doped titania so that the electrostatic stabilization can be realized. Thus far, we have explained the mechanisms of various coloring by building bandgap structures phase by phase. Simultaneously, we inferred the synergetic effects of crystal phase and dopants state and amount influence the final apparent colors of BN-TiO_2.

The photoexcitation relates to the wide absorption around 400–750 nm. In order to control and turn the color exactly, we applied an oxidation process at 700°C for 1 h in air before nitridation (called pre-oxidation, and the related samples were denoted as BNAO_*y*, BNRO_*y* and BNBO_*y*, *y* is the nitridation time, h) to increase the brightness of BN-TiO_2 samples. Fig. 5 shows the comparison of UV-vis light absorption behaviors between as-prepared B-TiO_2 (solid lines) and pre-oxidated BAO, BRO, and BBO (the dash lines), together with their UV-vis absorption spectra and related optical graphs of corresponding samples of BNAO, BNRO, and BNBO series samples, respectively.

As expected, the pre-oxidation makes it possible to weaken the background absorption efficiently (Fig. 5(a)), accordingly, the color of B-TiO_2 changes from gray to almost white. To keep in line with the previous synthesis method, 1 h nitridation was carried out firstly in an attempt to judge how the color change if the deficiencies become less in amount. In the case of BNAO_1 (Fig. 5(b)), the absorption to blue light strengthens lightly and results in a pale-yellow color, which is very different from that wide and strong absorption that appeared in BN-Ana (BNA_60 and BNA600). With the increase of nitridation time to 2 or 3 h, the absorption onset

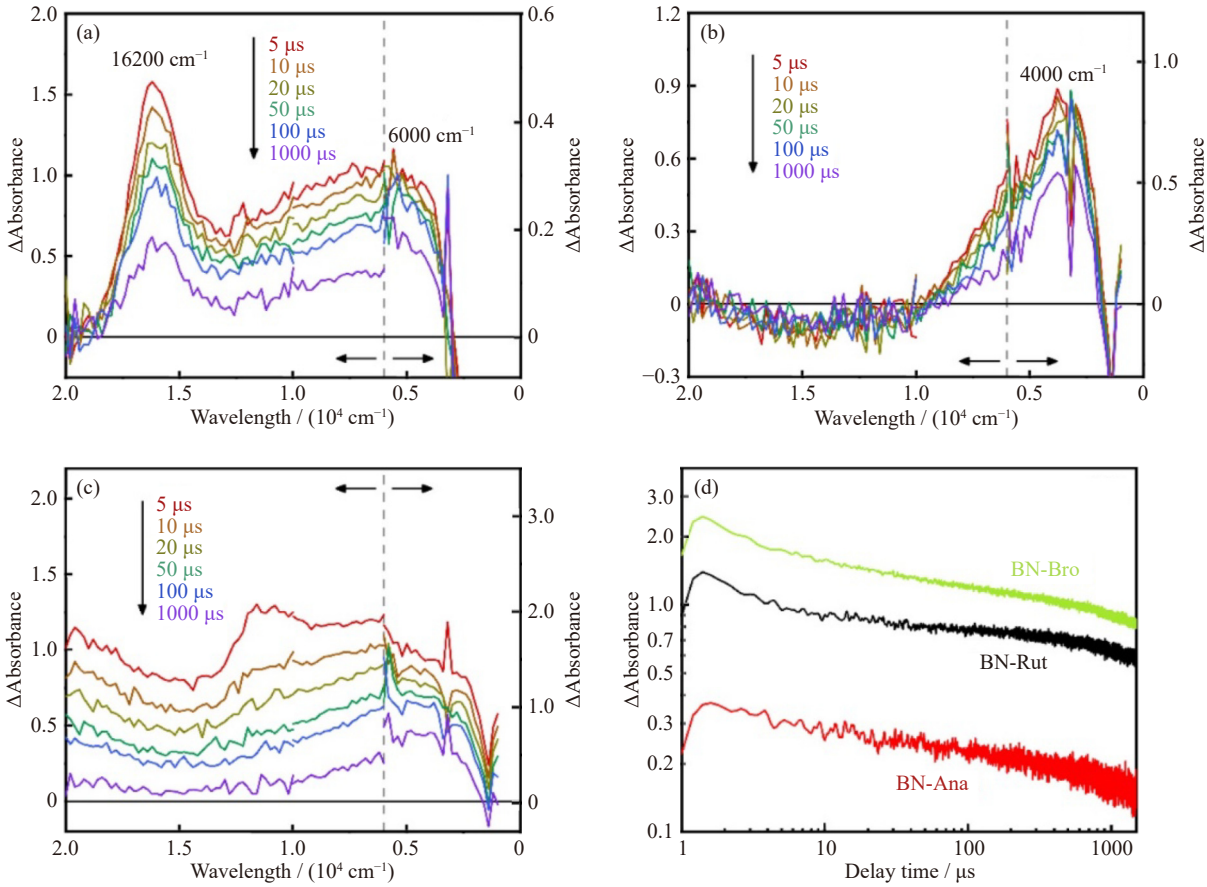

Fig. 4. Transient absorption spectra of (a) BN-Ana, (b) BN-Rut, and (c) BN-Bro collected after pumping with a 450 nm nanosecond laser at a delay time of 5–1000 μs. These spectra at 20000–6000 cm^{-1} and 6000–1000 cm^{-1} were measured with diffuse-reflection mode and transmission mode, respectively. (d) Dynamic change of the signal at k_{probe} = 4000 cm^{-1} as a function of pump-probe delay time (λ_{pump} = 450 nm).

gradually redshifts and the color turns to dark-red, as the optical graphs show. Based on the above, we inferred the effects of pre-oxidation for anatase-base BN-TiO_2 are brightening the color by reducing the Ti^{3+} states. It is worthwhile to note that a three-stage absorption is rarely formed in BNAO_3 (Fig. 5(b–i)). It is reasonable to consider that the bandgap structures of BNAO are further modified because of the pre-oxidation. For BNRO_*y* and BNBO_*y* samples, rather than evidently triggering the shift of absorption peak, the prolongation of nitridation time merely affects the intensities of original absorption and leads to darker colors. The same tendency has been reported recently by Bjelajaca *et al.* [42]. Pre-oxidation can result in much lower visible light sensitivity regardless of whether the N concentration is equivalent to the sample without pre-oxidation treatment. To make it easy to compare the color deviations between pre-oxidated samples with various nitridation times, the digitization of apparent color is implemented by calculating the values of color hue (h°) in terms of CIE L*a*b* coordinate. The vigorous changes of h° (76, 55, and 34 correspond to 1, 2, and 3 h nitridation) collected in Table S2 sufficiently express the distinctive color changes of BNAO_*y* samples when the nitridation time is prolonged. As for BNRO or BNBO, the almost unchanged hue and gradually decreased brightness contribute to the deepening inside the same color tone, as the inserts presented. The relevant L*a*b* coordinates of each pre-oxidated sample were recorded in Fig. S3.

3.2. Photocatalytic activity

Likewise, the light-driven NO decomposition experiments were carried out again on BNA, BNR, and BNB series samples. 450 W mercury lamp was applied as a light source. Three kinds of wavelengths (>510, >400, and >290 nm) were filtrated by cutoff filters. The light with a wavelength of >510 nm simulates blue light-free visible light, >400 nm responds to visible light, and >290 nm equals to ultraviolet included visible light (UV+vis). As expressed in Fig. 6, the brookite-based BN-TiO_2 plays the best performance in all three wave ranges and anatase or rutile phase BN-TiO_2 is passive. Else, we further analyze the effects of nitridation time (30, 60, and 120 min), and the effort of nitridation temperatures (500–700°C) with regard to anatase, rutile, and brookite, respectively. The difference between the samples with diverse nitridation time is so negligible that the nitridation time seems no exact effects on varying the photocatalytic activity of BN-TiO_2. These approximate deNO_x capacities are highly coupled with those restricted changes in optical features (Fig. 3). Under different nitridation temperature, for anatase-based BN-TiO_2, higher nitridation temperature lower UV+vis light (>290 nm) caused photodegradation activities. Besides,

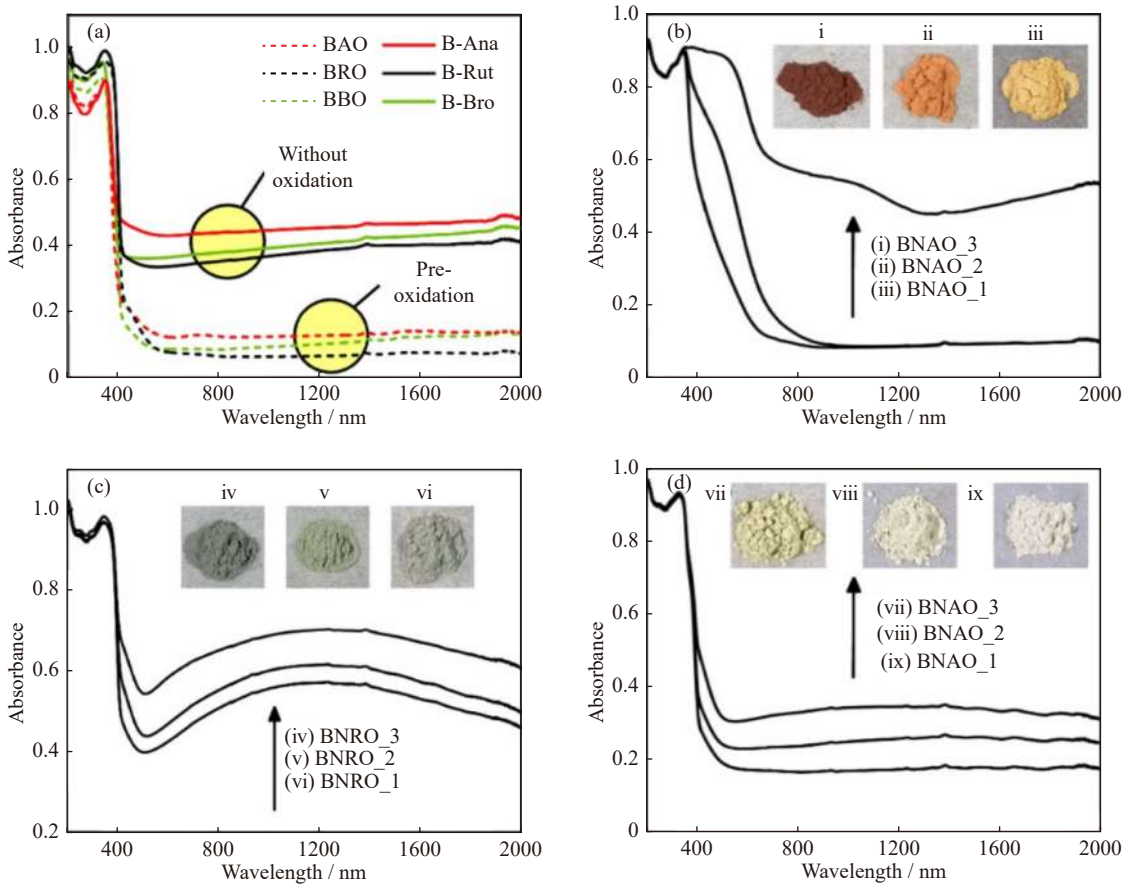

Fig. 5. (a) Comparison of UV-vis light absorption behaviors between as-prepared B-TiO_2 (solid lines) and pre-oxidated BAO, BRO, and BBO (the dash lines); (b–d) UV-vis absorption spectra and related optical graphs of BNAO, BNRO, and BNBO series samples, respectively.

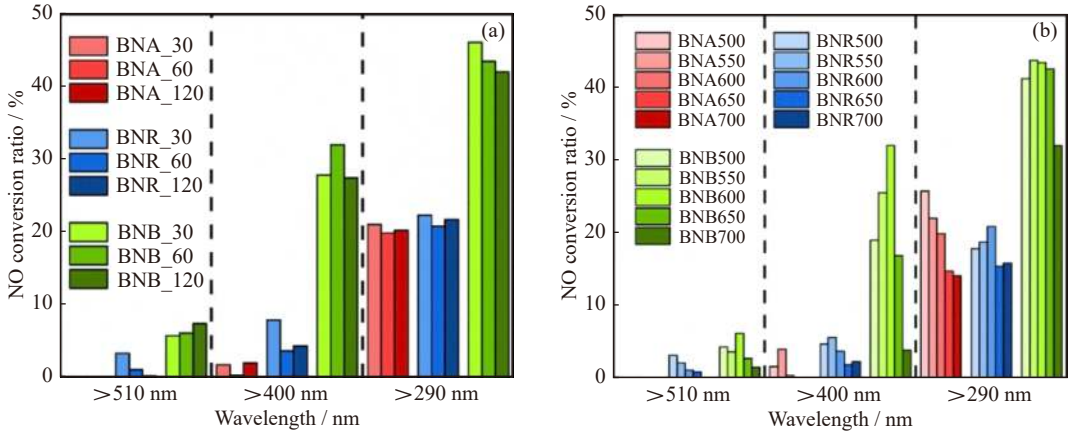

Fig. 6. Light-driven NO decomposition ability of the samples synthesized (a) under nitridation at 600°C for 30–120 min and (b) under nitridation at 500–700°C for 60 min. The columns are grouped by crystal phases. Red is for anatase, blue is for rutile, and green is for brookite. 450 W mercury lamp is used as the light source. The wavelength of >510, >400, and >290 nm is selected to simulate blue light-free visible light, visible light, and UV+vis light, respectively.

the inertness to visible light remains still. Simultaneously, a similar trend has been repeated in the case of rutile-based samples. The deNO_x capacities decrease step by step as temperatures go up to 700°C, except BNR600 shows the best activity under UV+vis light radiation. Brookite-based samples exhibit outstanding activities among three phases conforming to the aforementioned consequence. By comparing five BNB samples with each other, the one treated at 600°C seems optimal. However, when the temperature is higher than 650°C, a process of inactivation can be observed clearly, especially BNB_700 hardly shows comparable activity to visible light. Basically, the photoactivity of all three kinds of BN-TiO_2 will decline if the nitridation temperature tends to be higher. The excessive amount of Ti^{3+} defects originating from N doping [34] is harmful to the ultimate deNO_x efficiency by raising the opportunities for recombination [43].

Fig. S4 shows the photocatalytic activities of the pre-oxid-

ated samples. By applying the pre-oxidation treatment, the deNO$_x$ photocatalytic activity of brookite also decreased to almost the same level of anatase and rutile phases, indicating the possibility for cosmetic applications. Fig. S5 shows the photocatalytic activities of the as-prepared BN-TiO$_2$ samples, together with those of Degussa P25 as a reference. Also, the photocatalytic activity stability of BN-Bro was further investigated using five times recycling experiments under irradiation of visible light wavelength ($\lambda \geq 400$ nm). The according results are depicted in Fig. S5(b). The NO conversion ratio decreased from the initial 32.0% to the terminal 17.9% after five cycles, dropping by nearly 44%. In addition, there is a noticeable deactivation (NO concentration rises again after arriving at a minimum point) within every cycle. Intrinsically, these two kinds of inactivation individually attribute to different mechanisms. Undesired repeatability generally deals with surface destruction [44] or the degeneration of active sites [45]. For the inactivation within one experiment, the recombination of photoinduced electrons is the main reason [46]. Despite the comparable photocatalytic activity of BN-Bro, its instability limits its practical application as a visible light-driven photocatalyst. Also, BN-Ana and BN-Rut are not suitable for photocatalysts because of their inertness.

It was found that different phases of the BN-TiO$_2$ possessed different deNO$_x$ photocatalytic activity. Both of BN-Ana and BN-Rut are inert under light irradiation, while the BN-Bro shows better photocatalytic performance than that of Degussa P25. Although the colorful titania-based materials shows limited deNO$_x$ photocatalytic activity compared with other photocatalytic materials (Table S3, under complete same characterization conditions), the low photocatalytic activity and apparent colorful colors make the as-prepared BN-TiO$_2$ as pigments and cosmetic materials possible, in which cases the low and controllable photocatalytic activity is preferred. In conclusion, the sample (especially the anatase and rutile phase) without high photoactivity but features of coloring is reasonable enough to be treated as a unique pigment or cosmetic material.

4. Conclusion

The color of as-obtained BN-TiO$_2$ changes based on their different phase. The various BN-TiO$_2$ show specific red color (BN-Ana), yellow-green (BN-Bro), and cyan-green (BN-Rut), indicating their different visible light absorption ability. The onset of the BN-Ana absorption extends to about 750 nm. Because of its strong absorption of blue light, the BN-Ana shows the red base color, while the cyan-green BN-Rut presents a rare strong absorption during the near-infrared (NIR) area. The reasons for varied colorations are speculated as to the different electronic band configurations, which are greatly affected by the interaction between B and N dopants as well as the amount of each impurity. The different phase structures of the BN-TiO$_2$ shows different photocatalytic deNO$_x$ activity. Both of the BN-Ana and BN-Rut titania are stable under light irradiation, however, the BN-Bro titania possesses the most attractive NO degradation capacity either under visible light or ultraviolet light (UV) illumination, even performs better than that of Degussa P25 titania. The low photocatalytic activity and different color of the as-obtained BN-TiO$_2$ titania indicates their great potential and possibility for using as novel pigments and cosmetic raw materials.

Acknowledgements

This research was supported by the KOSÉ Cosmetology Research Foundation, the Japan Society funded the present work for the Promotion of Science (JSPS) Grant-in-Aid for Scientific Research (Nos. 16H06439 and 20H00297) and the Dynamic Alliance for Open Innovation Bridging Human, Environment and Materials in Network Joint Research Center for Materials and Devices.

Conflict of Interest

Wenbin Cao and Shu Yin are editorial board members for this journal and were not involved in the editorial review or the decision to publish this article. The authors declare that they have no known competing financial interests or personal relationships that could have appeared to influence the work reported in this paper.

Supplementary Information

The online version contains supplementary material available at https://doi.org/10.1007/s12613-022-2573-6.

References

[1] P. Zhang, S. Yin, and T. Sato, Synthesis of high-activity TiO$_2$ photocatalyst via environmentally friendly and novel microwave assisted hydrothermal process, *Appl. Catal. B*, 89(2009), No. 1-2, p. 118.

[2] S. Yin and Y. Asakura, Recent research progress on mixed valence state tungsten based materials, *Tungsten*, 1(2019), No. 1, p. 5.

[3] A. Hermawan, N.L.W. Septiani, A. Taufik, B. Yuliarto, and S. Yin, Advanced strategies to improve performances of molybdenum-based gas sensors, *Nano-Micro Lett.*, 13(2021), No. 1, art. No. 207.

[4] J. Cao, T. Hasegawa, Y. Asakura, *et al*., Synthesis and color tuning of titanium oxide inorganic pigment by phase control and mixed-anion co-doping, *Adv. Powder Technol.*, 33(2022), No. 5, art. No. 103576.

[5] S. Yin, Creation of advanced optical responsive functionality of ceramics by green processes, *J. Ceram. Soc. Jpn.*, 123(2015), No. 1441, p. 823.

[6] Y. Xue and S. Yin, Element doping: A marvelous strategy for pioneering the smart applications of VO$_2$, *Nanoscale*, 14(2022), No. 31, p. 11054.

[7] A. Hermawan, T. Amrillah, A. Riapanitra, W.J. Ong, and S. Yin, Prospects and challenges of MXenes as emerging sensing materials for flexible and wearable breath-based biomarker diagnosis, *Adv. Healthcare Mater.*, 10(2021), No. 20, art. No. 2100970.

[8] S. Yin and T. Hasegawa, Morphology control of transition metal oxides by liquid-phase process and their material development, *KONA Powder Part. J.*, 40(2023), p. 94.

[9] A. Hermawan, H. Son, Y. Asakura, T. Mori, and S. Yin, Syn-

thesis of morphology controllable aluminum nitride by direct nitridation of γ-AlOOH in the presence of N_2H_4 and their sintering behavior, *J. Asian Ceram. Soc.*, 6(2018), No. 1, p. 63.
[10] A. Hermawan, Y. Asakura, and S. Yin, Morphology control of aluminum nitride (AlN) for a novel high-temperature hydrogen sensor, *Int. J. Miner. Metall. Mater.*, 27(2020), No. 11, p. 1560.
[11] S. Chu and A. Majumdar, Opportunities and challenges for a sustainable energy future, *Nature*, 488(2012), No. 7411, p. 294.
[12] A.G. Olabi, M. Mahmoud, B. Soudan, T. Wilberforce, and M. Ramadan, Geothermal based hybrid energy systems, toward eco-friendly energy approaches, *Renewable Energy*, 147(2020), p. 2003.
[13] N.L. Panwar, S.C. Kaushik, and S. Kothari, Role of renewable energy sources in environmental protection: A review, *Renewable Sustainable Energy Rev.*, 15(2011), No. 3, p. 1513.
[14] G. Liu, L.C. Yin, J. Wang, *et al*., A red anatase TiO_2 photocatalyst for solar energy conversion, *Energy Environ. Sci.*, 5(2012), No. 11, p. 9603.
[15] G. Liu, J. Pan, L. Yin, *et al*., Heteroatom-modulated switching of photocatalytic hydrogen and oxygen evolution preferences of anatase TiO_2 microspheres, *Adv. Funct. Mater.*, 22(2012), No. 15, p. 3233.
[16] D. Wang, S. Wang, B. Li, Z. Zhang, and Q. Zhang, Tunable band gap of N, V co-doped Ca:TiO_2B ($CaTi_5O_{11}$) for visible-light photocatalysis, *Int. J. Hydrogen Energy*, 44(2019), No. 10, p. 4716.
[17] X. Li, Y. Liu, P. Yang, and Y. Shi, Visible light-driven photocatalysis of W, N co-doped TiO_2, *Particuology*, 11(2013), No. 6, p. 732.
[18] S. Komatsuda, Y. Asakura, J.J.M. Vequizo, A. Yamakata, and S. Yin, Enhanced photocatalytic NO_x decomposition of visible-light responsive F-TiO_2/(N, C)-TiO_2 by charge transfer between F-TiO_2 and (N, C)-TiO_2 through their doping levels, *Appl. Catal. B*, 238(2018), p. 358.
[19] H.T. Gao, Y.Y. Liu, C.H. Ding, D.M. Dai, and G.J. Liu, Synthesis, characterization, and theoretical study of N, S-codoped nano-TiO_2 with photocatalytic activities, *Int. J. Miner. Metall. Mater.*, 18(2011), No. 5, p. 606.
[20] N. Pienutsa, K. Yannawibut, J. Phattharaphongmanee, O. Thonganantakul, and S. Srinives, Titanium dioxide-graphene composite electrochemical sensor for detection of hexavalent chromium, *Int. J. Miner. Metall. Mater.*, 29(2022), No. 3, p. 529.
[21] H.H. Wang, W.X. Liu, J. Ma, *et al*., Design of $(GO/TiO_2)_N$ one-dimensional photonic crystal photocatalysts with improved photocatalytic activity for tetracycline degradation, *Int. J. Miner. Metall. Mater.*, 27(2020), No. 6, p. 830.
[22] Z. Gu, Z. Cui, Z. Wang, *et al*., Carbon vacancies and hydroxyls in graphitic carbon nitride: Promoted photocatalytic NO removal activity and mechanism, *Appl. Catal. B*, 279(2020), art. No. 119376.
[23] C. Noda, Y. Asakura, K. Shiraki, A. Yamakata, and S. Yin, Synthesis of three-component C_3N_4/rGO/C-TiO_2 photocatalyst with enhanced visible-light responsive photocatalytic deNO activity, *Chem. Eng. J.*, 390(2020), art. No. 124616.
[24] Z. Gu, B. Zhang, Y. Asakura, *et al*., Alkali-assisted hydrothermal preparation of g-C_3N_4/rGO nanocomposites with highly enhanced photocatalytic NO_x removal activity, *Appl. Surf. Sci.*, 521(2020), art. No. 146213.
[25] H. Li, S. Yin, Y. Wang, and T. Sato, Current progress on persistent fluorescence-assisted composite photocatalysts, *Funct. Mater. Lett.*, 6(2013), No. 6, art. No. 1330005.
[26] X. Wu, S. Yin, Q. Dong, *et al*., UV, visible and near-infrared lights induced NO_x destruction activity of (Yb, Er)-$NaYF_4$/C-TiO_2 composite, *Sci. Rep.*, 3(2013), art. No. 2918.
[27] X. Wu, S. Yin, Q. Dong, and T. Sato, Blue/green/red colour emitting up-conversion phosphors coupled C-TiO_2 composites with UV, visible and NIR responsive photocatalytic performance, *Appl. Catal. B*, 156-157(2014), p. 257.
[28] R. Asahi, T. Morikawa, T. Ohwaki, K. Aoki, and Y. Taga, Visible-light photocatalysis in nitrogen-doped titanium oxides, *Science*, 293(2001), No. 5528, p. 269.
[29] H. Lin, L. Li, M. Zhao, *et al*., Synthesis of high-quality brookite TiO_2 single-crystalline nanosheets with specific facets exposed: Tuning catalysts from inert to highly reactive, *J. Am. Chem. Soc.*, 134(2012), No. 20, p. 8328.
[30] A. Inagawa and N. Uehara, Development of colorimetric analysis with smartphones-captured images based on RGB-spectrum conversion methods, *Bunseki Kagaku*, 69(2020), No. 12, p. 693.
[31] Japanese Industrial Standard, *Fine ceramics (advanced ceramics, advanced technical ceramics)– Test Method for Air Purification Performance of Photocatalytic Materials–Part* 1: *Removal of Nitric Oxide*, Japanese Standards Association, Tokyo, 2016.
[32] V.V. Ivanov, I.A. Blokhina, and S.D. Kirik, Synthesis of TiB_2 by carbothermal reduction of oxides at lowered temperatures, *Russ J. Appl. Chem.*, 86(2013), No. 11, p. 1650.
[33] A. Ghanbari, M. Sakaki, A. Faeghinia, M.S. Bafghi, and K. Yanagisawa, Synthesis of nanocrystalline TiB_2 powder from TiO_2, B_2O_3 and Mg reactants through microwave-assisted self-propagating high-temperature synthesis method, *Bull. Mater. Sci.*, 39(2016), No. 4, p. 925.
[34] E. Finazzi, C. Di Valentin, and G. Pacchioni, Boron-doped anatase TiO_2: Pure and hybrid DFT calculations, *J. Phys. Chem. C*, 113(2009), No. 1, p. 220.
[35] Y. Du, Z. Wang, H. Chen, H.Y. Wang, G. Liu, and Y. Weng, Effect of trap states on photocatalytic properties of boron-doped anatase TiO_2 microspheres studied by time-resolved infrared spectroscopy, *Phys. Chem. Chem. Phys.*, 21(2019), No. 8, p. 4349.
[36] C. Di Valentin, G. Pacchioni, A. Selloni, S. Livraghi, and E. Giamello, Characterization of paramagnetic species in N-doped TiO_2 powders by EPR spectroscopy and DFT calculations, *J. Phys. Chem. B*, 109(2005), No. 23, p. 11414.
[37] Z. Zhang, X. Wang, J. Long, Q. Gu, Z. Ding, and X. Fu, Nitrogen-doped titanium dioxide visible light photocatalyst: Spectroscopic identification of photoactive centers, *J. Catal.*, 276(2010), No. 2, p. 201.
[38] T. Kanazawa, K. Kato, R. Yamaguchi, *et al*., Cobalt aluminate spinel as a cocatalyst for photocatalytic oxidation of water: Significant hole-trapping effect, *ACS Catal.*, 10(2020), No. 9, p. 4960.
[39] A. Miyoshi, K. Kato, T. Yokoi, *et al*., Nano *vs*. bulk rutile TiO_2: N, F in Z-scheme overall water splitting under visible light, *J. Mater. Chem. A*, 8(2020), No. 24, p. 11996.
[40] M. Landmann, E. Rauls, and W.G. Schmidt, The electronic structure and optical response of rutile, anatase and brookite TiO_2, *J. Phys. Condens. Matter*, 24(2012), No. 19, art. No. 195503.
[41] C. Di Valentin, G. Pacchioni, and A. Selloni, Origin of the different photoactivity of N-doped anatase and rutile TiO_2, *Phys. Rev. B*, 70(2004), No. 8, art. No. 085116.
[42] A. Bjelajac, R. Petrović, M. Popović, *et al*., Doping of TiO_2 nanotubes with nitrogen by annealing in ammonia for visible light activation: Influence of pre- and post-annealing in air, *Thin Solid Films*, 692(2019), art. No. 137598.
[43] H.M. Hwang, S. Oh, J.H. Shim, *et al*., Phase-selective disordered anatase/ordered rutile interface system for visible-light-driven, metal-free CO_2 reduction, *ACS Appl. Mater. Interfaces*, 11(2019), No. 39, p. 35693.
[44] G. Colón, M.C. Hidalgo, and J.A. Navio, Photocatalytic deactivation of commercial TiO_2 samples during simultaneous photoreduction of Cr(VI) and photooxidation of salicylic acid, *J. Photochem. Photobiol. A*, 138(2001), No. 1, p. 79.
[45] H. Yu, L. Liu, X. Wang, P. Wang, J. Yu, and Y. Wang, The dependence of photocatalytic activity and photoinduced self-stability of photosensitive AgI nanoparticles, *Dalton Trans.*, 41(2012), No. 34, p. 10405.
[46] X. Chen, L. Liu, P.Y. Yu, and S.S. Mao, Increasing solar absorption for photocatalysis with black hydrogenated titanium dioxide nanocrystals, *Science*, 331(2011), No. 6018, p. 746.